Volume 11 | Number 5 | 7 February 2019 | Pages 2093–2538

Nanoscale

rsc.li/nanoscale

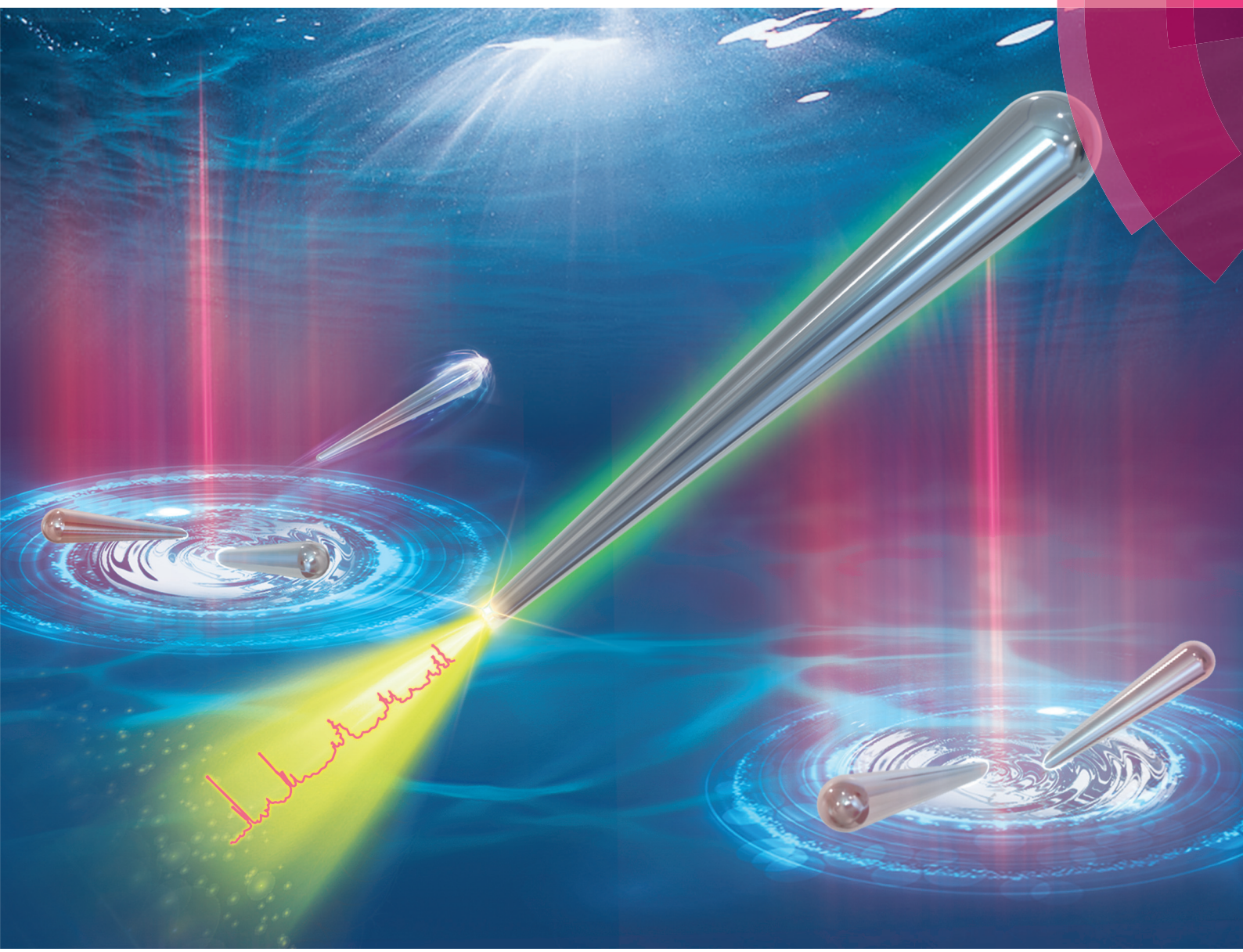

ISSN 2040-3372

ROYAL SOCIETY OF CHEMISTRY | Celebrating IYPT 2019

PAPER
Zhipeng Li *et al.*
Silver nano-needles: focused optical field induced solution synthesis and application in remote-excitation nanofocusing SERS

NCNST

Nanoscale

PAPER

View Article Online
View Journal | View Issue

Cite this: *Nanoscale*, 2019, **11**, 2153

Silver nano-needles: focused optical field induced solution synthesis and application in remote-excitation nanofocusing SERS†

Pan Li,[a] Deng Pan,[b] Longkun Yang,[a] Hong Wei,[c] Shuli He,[a] Hongxing Xu[b,d,e] and Zhipeng Li*[a]

Received 2nd September 2018,
Accepted 12th October 2018

DOI: 10.1039/c8nr07141a

rsc.li/nanoscale

Tapered metallic nanostructures that harbor surface plasmons are highly interesting for nanophotonic applications because of their waveguiding and field-focusing properties. Here, we developed a focused optical field induced solution synthesis for unique crystallized silver nano-needles. Under the focused laser spot, inhomogeneous Ag monomer concentration is created, which triggers the uniaxial growth of silver nanostructures along the radial direction with decreasing rate, forming nano-needle structures. These nano-needles are several micrometers long, with diameter attenuating from hundreds to tens of nanometers, and terminated by a sharp apex only a few nanometers in diameter. Moreover, nano-needles with atomically smooth surfaces show excellent performance for plasmonic waveguiding and unique near-field compression abilities. This nano-needle structure can be used for effective remote-excitation detection/sensing. We also demonstrate the assembling and picking up of nano-needles, which indicate potential applications in intracellular endoscopy, high resolution scanning tips, on-chip nanophotonic devices, *etc*.

1. Introduction

Noble metal nanostructure supporting surface plasmon polaritons (SPPs) have shown remarkable ability to confine and manipulate light at the nanometer length scale.[1–4] Benefiting from the state-of-the-art synthetic chemistry and nanolithography, various plasmonic analogues of macroscale optical components have been obtained to bridge the gap between the electronics and traditional photonics.[5–15] A particular focus in these efforts has been to realize functional tapered nanostructures, such as metallic tapered grooves[16–18] and stripes[19–22] as well as conical and pyramidal tips.[23–28] These structures have both a high aspect ratio and tapered profile. This distinct morphologic feature enables the attractive functionality known as nanofocusing, that is, plasmons can be guided in these nanostructures and finally focused to the sharp apex to generate an enormous local field enhancement.[29–33] Fascinating nanofocusing applications such as high-resolution near-field optical microscopy[27,34–37] and ultrasensitive detection[38–41] have been realized. However, current approaches to realize tapered plasmonic nanostructures have relied on sophisticated fabrication techniques, such as electron beam lithography and focused ion beam milling. It inevitably introduces inherent surface roughness that substantially degrades the optical performance.[42–44] A solution is to use chemically synthesized nanostructures that usually have crystallized characters and excellent optical responses. Although versatile metallic nanomaterials including silver and gold spheres,[45,46] cubes,[47,48] polyhedra,[49,50] rods[51–53] and wires[54–56] can be controllably synthesized, until now there is still a lack of synthesis approaches for high aspect ratio tapered nanostructures with atomically smooth surfaces.

In this work, we develop an inhomogeneous optical field induced reduction method to synthesize unique silver nano-needles (NNs) with several micrometers in length and transverse diameters attenuating from hundreds to several nanometers (for the dynamic synthesis process see Movie S1†). Verified by the observation of non-uniform SPP beats, these NNs are excellent SPP waveguides with a divergent effective refractive index for plasmon modes, fulfilling the requirement

[a]*The Beijing Key Laboratory for Nano-Photonics and Nano-Structure (NPNS), Center for Condensed Matter Physics, Department of Physics, Capital Normal University, Beijing 100048, P.R. China. E-mail: zpli@cnu.edu.cn*
[b]*School of Physics and Technology, Wuhan University, Wuhan 430072, P. R. China*
[c]*Beijing National Laboratory for Condensed Matter Physics, Institute of Physics Chinese Academy of Sciences, University of Physics Chinese Academy of Sciences, Collaborative Innovation Center of Quantum Matter, Beijing 100190, P. R. China*
[d]*The Institute for Advanced Studies, Wuhan University, Wuhan 430072, P. R. China*
[e]*Division of Solid State Physics/The Nanometer Structure Consortium, Lund University, Box 118, S-22100 Lund, Sweden*

†Electronic supplementary information (ESI) available. See DOI: 10.1039/c8nr07141a

of adiabatic nanofocusing.[31,33] Scanning near-field optical microscopy (SNOM) measurements visualize the effective compression of surface plasmons to the sharp end of NNs. Utilizing the unique nanofocusing ability, we demonstrated that the nano-needles can be used for effective remote-excitation surface-enhanced Raman scattering (SERS) detection and freely manipulated by an micromanipulator, which is promising for applications on constructing on-chip nanophotonic networks, high-resolution near-field optical microscopy[57,58] and ultrasensitive detection for sensing.[38,39] The growth mechanism can be understood by the competing growth of face-centered cubic (fcc) facets in the inhomogeneous growth environment created by the focused light field. These findings also demonstrate a promising possibility to synthesize functional nanostructures through the photo-chemical method by designing the optical field distribution.

2. Results and discussion

2.1 Photochemical synthesis of roughness-free silver nano-needles

Our experimental setup for the laser-induced synthesis of silver NNs is schematically shown in Fig. 1a (for details see the ESI†). A continuous wave laser (980 nm) was focused into the cell filled with reactant solution prepared by silver nitrate and sodium citrate. Silver ions in the aqueous solution can then be reduced under the laser spot due to the photochemical effect.[59–61] After 1 min irradiation, dense aggregates of Ag nanoparticles (NPs) with diameters ranging from 20 to 100 nm were generated in the area of the laser spot (Fig. 1b and c). Surprisingly, tens of NN structures were also observed on the outside of the laser spot. A close-up view of one of the needles (Fig. 1d) shows that it is 4.2 μm in length. And the transverse diameter gradually decreases from the thick end (D = 127 nm) to the thin end (D = 60 nm) with a gradient $D' = dD/dz \approx -0.02$ (Fig. 1e). At the thin termination, a larger gradient $D' \sim -0.9$ is found, generating a sharp apex with a size of only ~7 nm (inset in Fig. 1e). The thick end is terminated by a "big head" with a size of about ~170 nm. SEM images of other NNs are given in Fig. S1.† We monitored a typical growth process during laser illumination (see Fig. S2 and Movie S2† for details). It was found that the thin end was initially formed at a position close to the beam center, and the other end grew away from the beam center with increasing diameter. Finally, the needle was ejected out of the laser spot with a speed of ~17 μm s^{-1} and deposited on the substrate several micrometers from its initial position.

2.2 Growth mechanism of the silver nano-needles and controlled synthesis

To understand the growth mechanism, the crystallographic structures of the silver NNs were investigated by selected area electron diffraction (SAED) and high resolution transmission electron microscopy (HRTEM) measurements. As shown in Fig. 2, the characterized NN is 2.7 μm long with the transverse diameter attenuating from 80 to 40 nm, from which we can

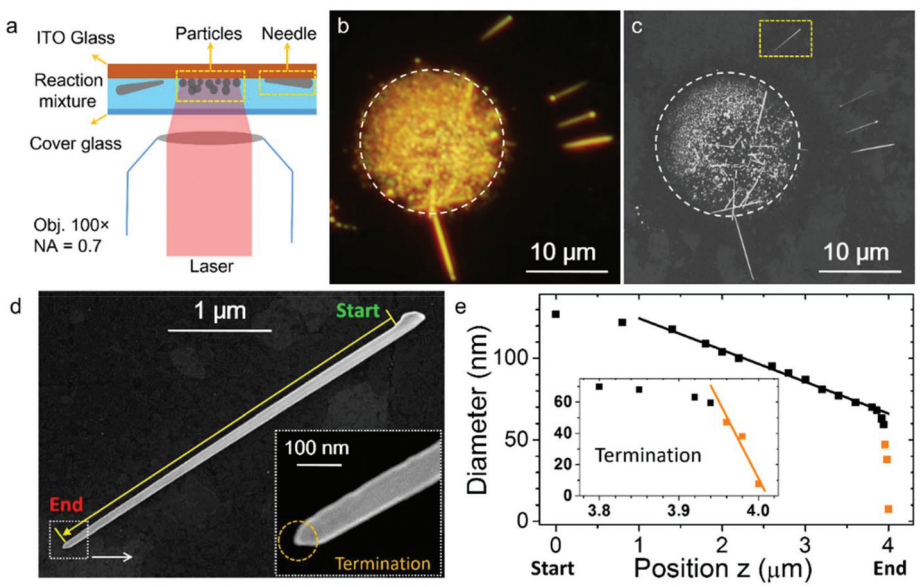

Fig. 1 Laser-induced synthesis of silver NNs. (a) Schematic of the experimental setup. The laser is 980 nm with a power of 120 mW. The reaction solution: silver nitrate and sodium citrate with the respective concentrations of 5 mM and 7 mM in a volume ratio of 1 : 1. (b) Dark-field optical image of the products. The white circle indicates the size of the laser spot. (c) SEM image of the products shown in (b). (d) Close-up of a nano-needle indicated by the yellow square in (c). The yellow line indicates the z axis along the needle. Inset: Zoomed view of the needle termination. (e) Transverse diameter as a function of positions along the needle (z axis) from the start point to the end indicated in (d). The black line is a linear fit between 1.4 and 3.8 μm. The inset shows the shrinking of the diameter at the sharp apex, and the orange line is a linear fit of the points closest to the apex.

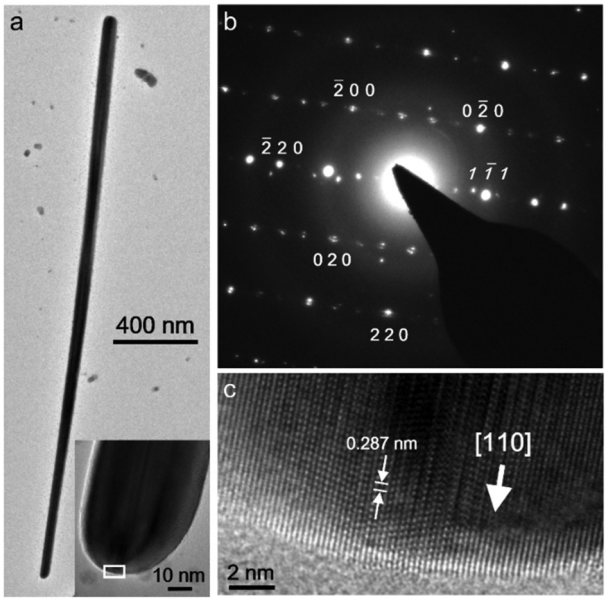

Fig. 2 HRTEM analysis of the silver NN. (a) Low magnification TEM image of a silver NN. The inset shows the zoomed view of the thinner end. (b) The corresponding SAED pattern from the thinner end. (c) HRTEM image of the square-enclosed region in the inset of (a).

find that the NN is well crystallized and has an atomically smooth surface. Details of the thinner end are shown in the inset of Fig. 2a. In the corresponding SAED pattern (Fig. 2b), most of the spots can be indexed to diffractions of two zone axes: [001] and [$\bar{1}$12], which suggests that the silver NN possesses a fcc twinned structure similar to the uniform nanowire synthesized by wet chemical methods.[54,55] Additionally, the SAED pattern also indicates that the NN has a longitudinal axis parallel to the [110] direction, which can be further confirmed by the HRTEM image in Fig. 2c. The X-ray diffraction and electron backscatter diffraction measurements were also performed (Fig. S3 and S4†), demonstrating consistent results with the SAED and HRTEM.

As is known, for a fcc structure in the absence of surfactants, the growth rate of the low-index crystallographic plane {110} is faster than that of the other two planes: {100} and {111}, because of the descending surface energies $\gamma_{\{110\}} > \gamma_{\{100\}} > \gamma_{\{111\}}$.[62] Hence, some initially formed Ag NPs can grow uniaxially along the [110] direction to form one dimensional nanostructures. Their diameter can be determined by the growth competition between the {110} facet and the other two.[63,64] The higher the growth rate of the {110} facet, the thinner the transverse diameter. Tian *et al.* also reported that thinner nanowires can be synthesized by improving the Ag monomer concentration to accelerate the growth of the {110} facet.[63] In our experiment, the Ag+ ions are photochemically reduced by focused laser field with the intensity decreasing exponentially along the radial direction (see Fig. S5†). So the reduced Ag monomer concentration decreases along the radial direction as well. Around the center of the laser spot, as the monomers in the stagnant solution (solution near the growth surface) are consumed, the monomers in the bulk solution with a relatively higher concentration can quickly diffuse to the {110} facet. Hence, the growth rate of {110} can significantly surpass that of the other two, allowing the NN to grow uniaxially with a small diameter. As one end of the needle gradually grows away from the center, however, it experiences a rapid decrease of monomer concentration due to the weakened laser intensity. Hence, the diffusion potential of the monomers from the bulk to stagnant solution is reduced, and the growth priority of the {110} facet is then substantially suppressed. This results in a larger transverse diameter and finally the preferential growth into a nanosphere structure through Ostwald ripening,[63] which is consistent with the observation of the needles with "big heads".

Here, the laser induced thermal effect on the Ag monomer concentration was also evaluated. By the fluorescence intensity ratio of the up-conversion nanomaterial,[65,66] the temperature gradient along the radial direction was measured (the Fig. S5†), where the difference between the spot center (~353 K) and edge (~323 K) was about 30 K. It was reported that, due to the angular mismatch of the five-fold twined crystallites and surface-free energy minimization, the higher the temperature, the bigger the diameter of the nanowire.[64] However, we found that the thinner end of the NN is always formed in the spot center (the Fig. S2†). It indicates that the gradient temperature is not the determinative reason for the tapered morphology. In our case, the concentrations of reactants are much higher than the one in the literature.[64] In such a circumstance, the photochemical reduction rather than temperature dominates the growth of the NNs. Consequently, it is the distribution of light intensity that determines the morphology of nanostructures. Another thermal effect that should be considered during the process is thermophoresis in the solution induced by laser irradiation.[67] It will lead to a pushing force exerted on the needles that can significantly increase as the needles grow. Once the pushing force finally overcomes the adhesion of the needle on the substrate, the needle can be suddenly ejected out of the laser spot. Nevertheless, the plasmon-induced effects, such as electric/magnetic resonance,[12,68] plasmoelectric potential,[69] hot electrons[70] and heating,[71] could also involve in the formation of nanostructures. However, as the wavelength of the laser (980 nm) in this work is relatively far from the resonance of silver nanostructures, light field distribution is still the key for the formation of the NNs.

We summarize the roles of the focused laser beam in the synthesis of silver NNs: (1) it induces the photochemical reduction of Ag+ ions, (2) it facilitates the uniaxial growth of needles by creating an inhomogeneous solution environment and (3) it leads to strong thermophoresis in the solution, which pushes the needles out of the laser spot. Here, we emphasize that the synthesis of NNs is a dynamic process. Needles may spin in the solution because of convection, which can flip over the NNs before they deposit on the substrate, thus resulting in a double-tapered structure as presented in

Fig. S1.† These interesting dynamic movements including NN ejection, flip-over and flowing back to the laser spot are presented in Movie S1,† and SEM images of the final products containing ~30 needles are presented in Fig. S6.†

Furthermore, we try to control the photochemical synthesis by changing the parameters such as light intensity, reactant concentrations and light distributions. First, we change the laser power while maintaining the reactant concentration used in Fig. 1. For the laser power below 100 mW, almost no NNs can be formed as shown in Fig. S7.† With the increase of the power from 100–150 mW, the yield of nano-needles increases. However, for laser power larger than 150 mW, the reactant solution will be evaporated which totally damages the reaction environment. On the other hand, under the same excitation conditions (120 mW), the reactant concentrations influence the NN yield significantly. As shown in Fig. 3a and b, the number of NNs increases from ~2 to ~40 when silver nitrate/sodium citrate concentrations increase from 4 mM/6 mM to 6 mM/8 mM. For a higher concentration, the reduction of Ag^+ ions could occur at room temperature even without laser illumination. The uncontrolled consumption of Ag^+ ions thus limits the yield of the NNs. The size of the laser spot is another key parameter for the NN synthesis. In our experiment, it extends up to ~10 μm providing an inhomogeneous solution environment large enough for NNs growth. For a larger photoexcitation area created by an objective with a magnification 20× (NA = 0.4), longer nano-needles can be obtained (Fig. 3c). Close-up views of two needles with longer lengths 13.3 μm ($dD/dz = -0.005$) and 8.5 μm ($dD/dz = -0.01$) are presented in Fig. 3d and e, respectively. Furthermore, by manipulating the relative position of the laser spot during the NN growth, we can actively control the morphologies of the synthesized needles. As shown in Fig. S8 and Movie S3,† a needle with a "big head" can be purposely synthesized by moving the growing needle to the edge of the laser spot, which can result from the Ostwald ripening induced by the sharp decrease of Ag monomer concentration in the edge of the laser spot.

2.3 Surface plasmon nanofocusing in silver NNs and remote-excitation detection

In light of the tapered shape and atomically smooth surfaces of the NNs, we demonstrate the potential use as a nanofocusing and remote-excitation source. Fig. 4a shows a SEM image of the investigated needle with a length of 6.4 μm and a diameter attenuating from 220 to 75 nm. Launching the SPPs at the thicker end with longitudinal polarization (see the ESI†), a bright emission spot can be observed at the thin end of the needle (Fig. 4b). It has been previously reported that the damping of SPPs increases with decreasing diameter owing to

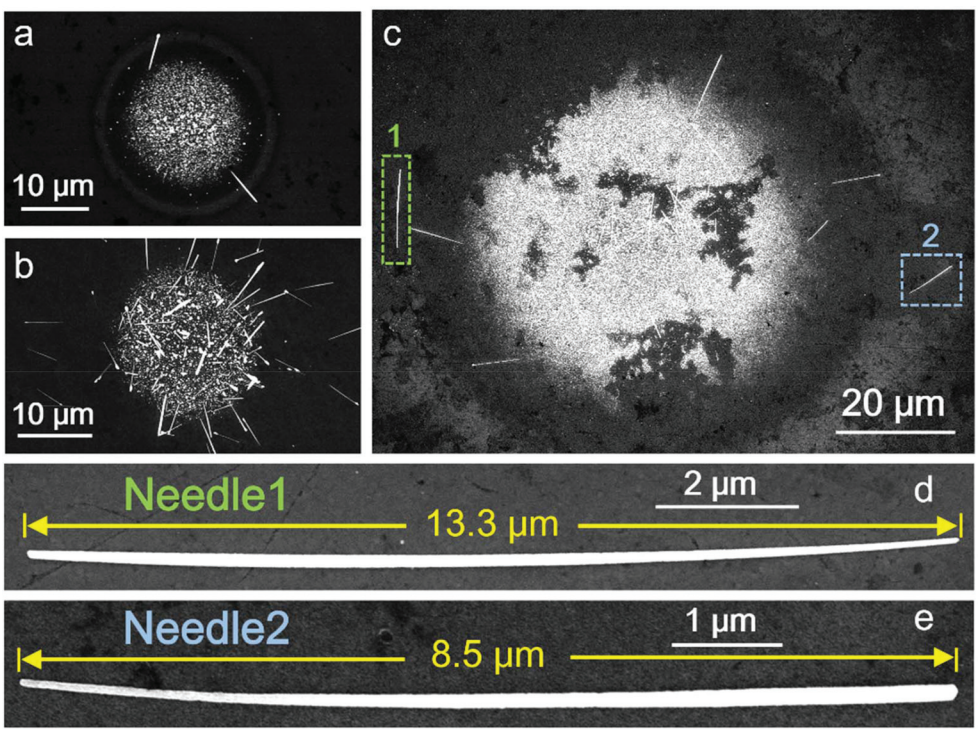

Fig. 3 Controlling yield and length of nano-needles by reactant concentrations and optical field. (a and b) SEM images showing the needle yield for lower and higher silver nitrate/sodium citrate concentrations than used previously: (a) 4 mM/6 mM and (b) 6 mM/8 mM. The two reactants were mixed in a volume ratio of 1 : 1, and the laser irradiation lasted for 60 s with an excitation power of 120 mW. (c) SEM image showing nano-needles formed in the laser spot with a larger photoexcitation area. The irradiation time was 90 s. Silver nitrate and sodium citrate reactants with respective concentrations of 6 mM and 8 mM were used in a volume ratio of 1 : 1. (d, e) Close-up views of the nano-needles, 1 and 2, indicated by the squares in (c).

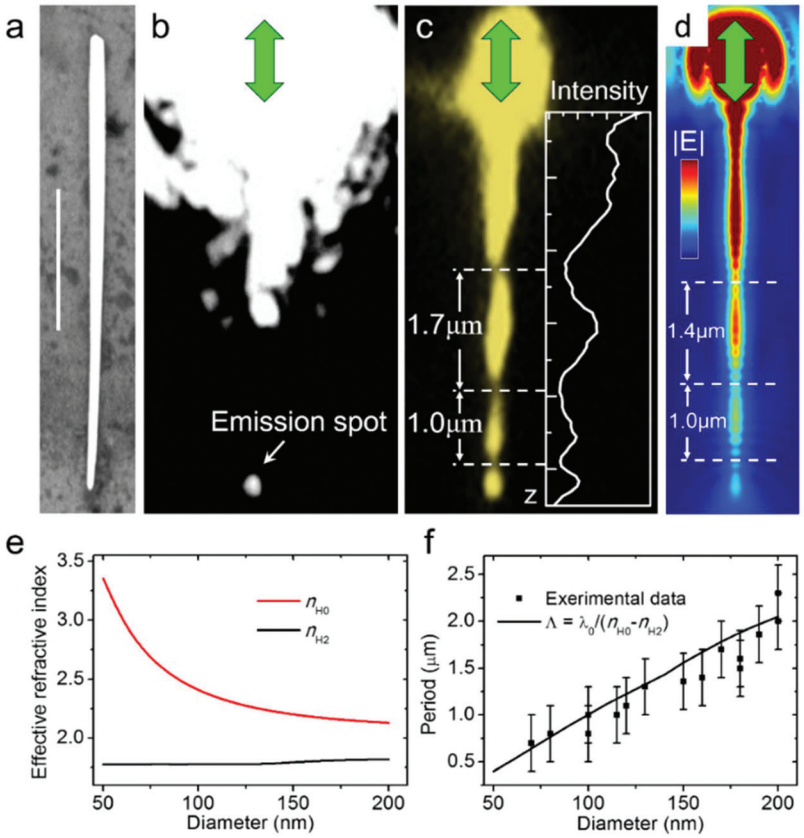

Fig. 4 Near-field distributions of SPPs in silver nano-needles. (a) SEM image of a silver nano-needle with a length of 6.4 μm and diameters of 220 nm and 75 nm at each end. The scale bar is 2 μm in length. (b) Optical image of the nano-needle under excitation of a focused laser beam (λ = 633 nm) at the thicker end. The incident polarization is marked by the green arrow. (c) QD emission image of the nano-needle. The inset shows the emission intensity profile along the nano-needle. (d) Calculated electric field distribution of propagating plasmons along the nano-needle with a length of 6.4 μm and diameters decreasing from 200 nm to 100 nm. The needle was excited at the thicker end by a focused laser polarized parallel to the longitudinal axis. Dark red and blue colors correspond to high and low intensities of the electric field, respectively. (e) Calculated effective refractive indices, n_{H_0} and n_{H_2}, for the H_0 and H_2 modes as a function of needle diameter. (f) Beat length as a function of needle diameter. The black curve represents the calculated result using the effective refractive indices in (e), and the dots represent the experimental data with the diameter being the average value for each observed beat length. The error bars are set as ±300 nm determined by the diffraction limit of the optical microscope.

the tighter field confinement.[72] Nevertheless, the needle shows the unique ability to channel SPPs over considerable distances to the very small end with a diameter of only several nanometers. To reveal the propagating properties of different plasmon modes in the NN, we visualized the near-field distribution along the needle by quantum dot- (QD) based local-field imaging. As shown in Fig. 4c, a quasiperiodic node-like field distribution along the needle was observed upon laser illumination. This near-field spatial modulation, or "beat", along the needle originates from the superposition of different propagating plasmon modes.[73] For cylindrical nanowires in uniform dielectric environments, the analytical eigenmode is indexed with azimuthal quantum number "m" which is an integer. Two lowest-order modes (m = 0 and m = −1) can be excited by the parallel polarized light.[72,74] For nanowires on a dielectric substrate, these modes will be changed to H_0 and H_2 modes, respectively, due to the break of cylindrical symmetry.[75]

H_0 is a longitudinal mode with electrons oscillating parallel to the wire axis, whereas H_2 is a transverse mode with electrons oscillating vertically to the substrate. The beat length, Λ, resulting from the constructive or destructive interference of the two modes is determined by the relation: $\Lambda = \lambda_0/(n_{H_0} - n_{H_2})$, where λ_0 is the wavelength under vacuum, and n_{H_0} and n_{H_2} are the effective refractive indices for the H_0 and H_2 modes, respectively. For nanowires with a uniform diameter, the beat length is constant, because the difference $n_{H_0} - n_{H_2}$ is invariant along the entire wire. For nano-needles, however, we found that the beat length changes along the longitudinal axis. As shown in Fig. 4c, the second beat near the excitation was ~1.7 μm long, covering part of the needle with the diameter attenuating from 200 to 140 nm, which corresponds to an average diameter of 170 nm. The third beat covering the thinner part of the needle with an average diameter of 115 nm was found to be shorter with a length of ~1.0 μm. We also show that chiral plasmons[76] can be formed by changing the incident polarizations (Fig. S9†).

Electromagnetic calculations of the plasmon modes were performed based on a finite element method (see the ESI†). Two plasmon modes, H_0 and H_2, can be excited upon parallel polarized excitation (Fig. S10†). The calculated electric field distribution resulted from the interference between the two plasmon modes, H_0 and H_2, is shown in Fig. 4d. The prominent experimental feature of decreasing beat lengths along the propagation direction was well reproduced. The decreasing beat length can be quantitatively evaluated by the relationship of the effective refractive indices to the diameter. As shown in Fig. 4e, the n_{H_0} increases rapidly with the decrease of the diameter, while the n_{H_2} remains almost constant. The beat lengths were then predicted with the relation $\Lambda = \lambda_0/(n_{H_0} - n_{H_2})$. As shown in Fig. 4f, the calculated beat lengths at different diameters are in good agreement with the experimental values. The effective refractive index for the H_0 mode that varies with the diameter ($n_{H_0} \propto 1/D$) has important implications for plasmon nanofocusing.[33] The focusing ability can be evaluated by the eikonal parameter, $\delta = |D'\mathrm{d}(k_0 n_{H_0})/\mathrm{d}D|$, where δ indicates how fast the SPP wavelength changes along the NN.[33] Generally, $\delta < 1$ is considered as an adiabatic focusing process. As an example, the main body of the needle shown in Fig. 1d exhibits an eikonal parameter of $\delta < 0.05$, which indicates an adiabatic regime of nanofocusing. With the tapering of NNs, the propagating SPPs become increasingly localized with negligible internal reflections and scattering. At the very end, where the adiabatic approximation is not applicable, δ could be larger than 1. As a consequence, the short and sharp termination of the needle will give rise to a high localization and enhancement of the near field.

To further visualize this process in silver NNs, near-field measurement using scattering-type SNOM (s-SNOM) is carried out. The 633 nm laser is focused on a metallized atomic force microscope (AFM) probe tip, where plasmons can be excited through the coupling between the tip and NNs. Plasmons propagating in the NNs are reflected at the termination of the needles and return to the AFM tip, which are then out-scattered to the far field. Optical pseudoheterodyne detection records the scattering field of the reflected plasmons interfering with the light directly scattered from the local coupling between the AFM tip and the NNs. By raster scanning the NN with the AFM probe, the topography and optical signal image beyond the diffraction limit can be obtained simultaneously (see the ESI† for details). A typical result is presented in Fig. 5a, where the topography measurement shows that the length of the NN is 5.7 μm and diameters attenuate from 120 nm to only 10 nm. In the corresponding optical image (Fig. 5b), a series of fringe patterns along the nano-needle is observed. Interestingly, it is found that the neighbor fringe spacing (ΔL) decreases gradually with the decrease of the transverse diameter (Fig. 5c). As plasmons returning to the tip experience twice the distance between the AFM tip and the needle termination, the ΔL is determined by the relation: $\Delta L = \lambda_0/(2n_{\mathrm{eff}})$,[77] where n_{eff} is the effective refractive index of the propagating plasmon mode. Then, the dependence of n_{eff} on the NN diameter can be extracted from the s-SNOM image.

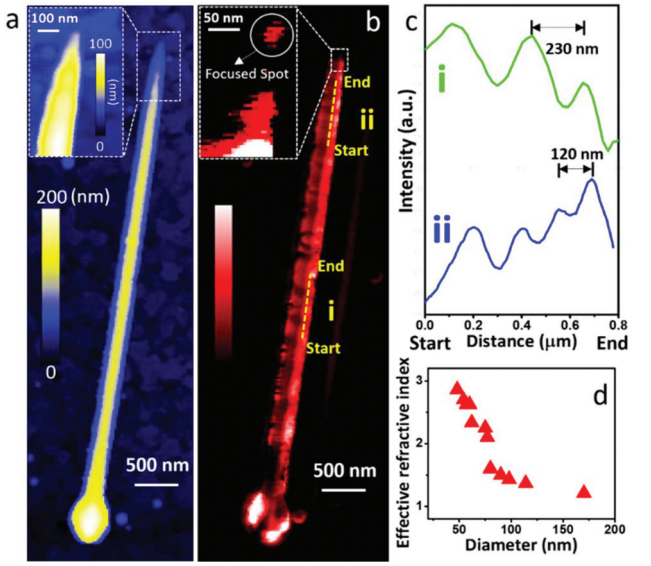

Fig. 5 Plasmon imaging of the silver nano-needle with s-SNOM. (a) AFM image of a silver nano-needle with a length of 5.7 μm. The enlarged view of the tip in the inset shows that the sharp apex is about 10 nm in size. (b) Plasmon image of the nano-needle shown in (a). The inset shows that the near field is highly focused at the apex. (c) The near-field intensity profiles along the cross lines i and ii in (b). (d) The experimentally measured effective refractive index as a function of nano-needle diameter.

Consistent with the result obtained by the QD imaging method, n_{eff} is proportional to the $1/D$ (Fig. 5d), fulfilling the requirement for adiabatic compression of surface plasmons.[33] Additionally, a highly focused spot with a size of ~20 nm (close to the optical resolution of s-SNOM measurement) is clearly observed at the sharp apex of the NN (inset of Fig. 5b), which indicates the effective nanofocusing process that compresses the near field to the volume far beyond the diffraction limit.

Through the adiabatic nanofocusing H_0 mode, the giant field at the tip of the NN structure is an ideal candidate for remote-excitation sources. As shown in Fig. 6, efficient remote-excitation nanofocusing SERS can be realized by launching propagating plasmons of the H_0 mode at the thick end and detecting Raman signals from the sharp tip. The detection limit of CV molecules can be as low as 10^{-9} M. At the same time, the Raman signal can hardly be observed under transverse polarized excitation, where non-nanofocusing mode H_2 is launched. Moreover, we also demonstrated that the nano-needles can be freely manipulated by a micromanipulator with an optical fiber. In Fig. S11,† a NN connection is successfully assembled. Plasmons launched in one NN can be effectively coupled into another one. We even pick up one NN and install it on a tapered fiber probe. Propagating SPPs can then be launched *via* the fiber probe by the "end-fired" configuration (Fig. S12†). It can be anticipated that these unique and easily manipulated NNs will have potential for intracellular SERS endoscopy, high resolution SERS imaging/sensing, building-blocks of integrated nanophotonic networks,[19] *etc.*

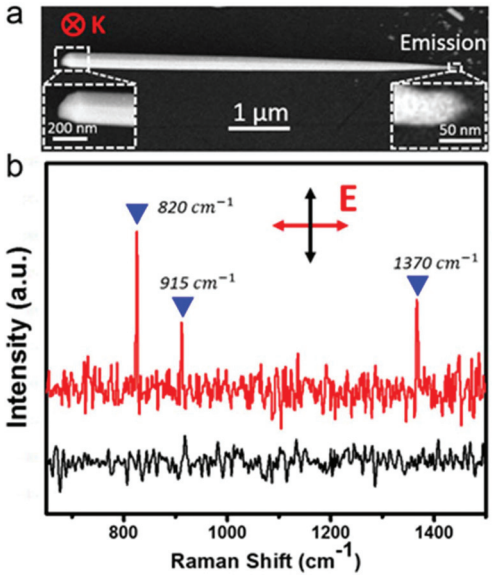

Fig. 6 Remote-excitation nanofocusing SERS detection of CV molecules. (a) SEM image of the nano-needle with a length of 5.5 μm. The transverse diameter gradually decreases from 200 to 40 nm, and the sharp apex at the thin end is about ~7 nm in size. The SPP propagation is launched at the thick end, and the remote-excitation nanofocusing SERS is detected at the thin end. (b) Remote-excitation nanofocusing SERS under the longitudinal (red) and transverse polarization (black).

3. Conclusions

In summary, we have reported a novel approach to realize ultra-smooth, silver NNs with a sharp tip, using focused optical field induced photochemical synthesis. The tapered morphology is the consequence of competing growth among the different facets of the fcc structure in the inhomogeneous growth environment created by the focused light field. These photochemically synthesized NNs can guide SPPs over a considerable distance and adiabatically compress the optical field to the sharp apex with a diameter only several nanometers, and thus can be a good candidate for remote-excitation sources. The detection sensitivity of CV for this remote-excitation nanofocusing SERS can be as low as 10^{-9} M. Moreover, we also demonstrate the assembling and picking up of NNs by a micromanipulator, which is promising for the applications of intracellular SERS endoscopy, high-resolution SERS imaging/sensing, building-blocks of integrated nanophotonic networks, *etc*. As for the synthesis technique, we have showed that the light field distribution can effectively tailor the morphology of chemically synthesized nanostructures. These results would also bring the methodology for controlled synthesis of plasmonic nanostructures by designed optical field distribution.

Conflicts of interest

There are no conflicts to declare.

Acknowledgements

Z. P. Li thanks Dr Qiang Li and Dr Zhiqiang Guan for the help on QD imaging and nano-needle manipulation experiments. This work was supported by the National Natural Science Foundation of China (Grant No. 11774245, 11674256, 11704266, 11422436, 11774413, 51571146, and 51771124), the Ministry of Science and Technology of China (Grant No. 2015CB932400), Fok Ying Tung Education Foundation (Grant No. 151010), Scientific Research Base Development Program of the Beijing Municipal Commission of Education, the Training Program of the Major Research Plan of Capital Normal University and the General Foundation of Beijing Municipal Commission of Education (Grant No. KM201810028006).

References

1 W. L. Barnes, A. Dereux and T. W. Ebbesen, *Nature*, 2003, **424**, 824–830.
2 M. L. Brongersma and V. M. Shalaev, *Science*, 2010, **328**, 440–441.
3 L. Shao, X. Zhuo and J. Wang, *Adv. Mater.*, 2017, **30**, e1704338.
4 T. Shegai, V. D. Miljković, K. Bao, H. Xu, P. Nordlander, P. Johansson and M. Käll, *Nano Lett.*, 2011, **11**, 706–711.
5 R. Kirchain and L. Kimerling, *Nat. Photonics*, 2007, **1**, 303–305.
6 T. Shegai, Z. P. Li, T. Dadosh, Z. Y. Zhang, H. X. Xu and G. Haran, *Proc. Natl. Acad. Sci. U. S. A.*, 2008, **105**, 16448–16453.
7 F. Hao, P. Nordlander, Y. Sonnefraud, P. Van Dorpe and S. A. Maier, *ACS Nano*, 2009, **3**, 643–652.
8 L. Falk, F. H. L. Koppens, C. L. Yu, K. Kang, N. de Leon Snapp, A. V. Akimov, M. H. Jo, M. D. Lukin and H. Park, *Nat. Phys.*, 2009, **5**, 475–479.
9 V. Giannini, A. I. Fernández-Domínguez, S. C. Heck and S. A. Maier, *Chem. Rev.*, 2011, **111**, 3888–3912.
10 T. Shegai, S. Chen, V. D. Miljković, G. Zengin, P. Johansson and M. Käll, *Nat. Commun.*, 2011, **2**, 481.
11 D. K. Lim, K. S. Jeon, H. M. Kim, J. M. Nam and Y. D. Suh, *Nat. Mater.*, 2010, **9**, 60–67.
12 N. J. Halas, S. Lal, W. S. Chang, S. Link and P. Nordlander, *Chem. Rev.*, 2011, **111**, 3913–3961.
13 S. Lal, J. H. Hafner, N. J. Halas, S. Link and P. Nordlander, *Acc. Chem. Res.*, 2012, **45**, 1887–1895.
14 P. Byers, H. Zhang, D. F. Swearer, M. Yorulmaz, B. S. Hoener, D. Huang, A. Hoggard, W. S. Chang, P. Mulvaney, E. Ringe, N. J. Halas, P. Nordlander, S. Link and C. F. Landes, *Sci. Adv.*, 2015, **1**, e1500988.
15 M. W. Knight, N. K. Grady, R. Bardhan, F. Hao, P. Nordlander and N. J. Halas, *Nano Lett.*, 2007, **7**, 2346–2350.
16 V. S. Volkov, S. I. Bozhevolnyi, S. G. Rodrigo, L. Martin-Moreno, F. J. Garcia-Vidal, E. Devaux and T. W. Ebbesen, *Nano Lett.*, 2009, **9**, 1278–1282.

17 T. Søndergaard, S. M. Novikov, T. Holmgaard, R. L. Eriksen, J. Beermann, Z. H. Han, K. Pedersen and S. I. Bozhevolnyi, *Nat. Commun.*, 2012, **3**, 969.
18 B. Desiatov, I. Goykhman and U. Levy, *Nano Lett.*, 2014, **14**, 648–652.
19 H. Choo, M. K. Kim, M. Staffaroni, T. J. Seok, J. Bokor, S. Cabrini, P. J. Schuck, M. C. Wu and E. Yablonovitch, *Nat. Photonics*, 2012, **6**, 838–844.
20 E. Verhagen, L. Kuipers and A. Polman, *Nano Lett.*, 2007, **7**, 334–337.
21 M. Schnell, P. Alonso-González, L. Arzubiaga, F. Casanova, L. E. Hueso, A. Chuvilin and R. Hillenbrand, *Nat. Photonics*, 2011, **5**, 283–287.
22 Y. Luo, M. Chamanzar, A. Apuzzo, R. Salas-Montiel, K. N. Nguyen, S. Blaize and A. Adibi, *Nano Lett.*, 2015, **15**, 849–856.
23 C. Ropers, C. C. Neacsu, T. Elsaesser, M. Albrecht, M. B. Raschke and C. Lienau, *Nano Lett.*, 2007, **7**, 2784–2788.
24 N. Talebi, W. Sigle, R. Vogelgesang, M. Esmann, S. F. Becker, C. Lienau and P. A. van Aken, *ACS Nano*, 2015, **9**, 7641–7648.
25 S. Jiang, Y. Zhang, R. Zhang, C. R. Hu, M. H. Liao, Y. Luo, J. L. Yang, Z. C. Dong and J. G. Hou, *Nat. Nanotechnol.*, 2015, **10**, 865–869.
26 R. Zhang, X. B. A. Zhang, H. F. Wang, Y. Zhang, S. Jiang, C. R. Hu, Y. Zhang, Y. Luo and Z. C. Dong, *Angew. Chem., Int. Ed.*, 2017, **56**, 5561–5564.
27 N. C. Lindquist, P. Nagpal, A. Lesuffleur, D. J. Norris and S. H. Oh, *Nano Lett.*, 2010, **10**, 1369–1373.
28 X. Kang, Q. Ruan, H. Zhang, F. Bao, J. Guo, M. Tang, S. Cheng and J. Wang, *Nanoscale*, 2017, **9**, 5879–5886.
29 M. I. Stockman, *Phys. Rev. Lett.*, 2004, **93**, 137404.
30 K. Gramotnev and S. I. Bozhevolnyi, *Nat. Photonics*, 2014, **8**, 13–22.
31 S. Berweger, J. M. Atkin, R. L. Olmon and M. B. Raschke, *J. Phys. Chem. Lett.*, 2012, **3**, 945–952.
32 S. R. Guo, N. Talebi, W. Sigle, R. Vogelgesang, G. Richter, M. Esmann, S. F. Becker, C. Lienau and P. A. van Aken, *Nano Lett.*, 2016, **16**, 6137–6144.
33 P. Groß, M. Esmann, S. F. Becker, J. Vogelsang, N. Talebi and C. Lienau, *Adv. Phys.: X*, 2016, **1**, 297–330.
34 C. C. Neacsu, S. Berweger, R. L. Olmon, L. V. Saraf, C. Ropers and M. B. Raschke, *Nano Lett.*, 2010, **10**, 592–596.
35 S. Berweger, J. M. Atkin, X. J. G. Xu, R. L. Olmon and M. B. Raschke, *Nano Lett.*, 2011, **11**, 4309–4313.
36 S. Schmidt, B. Piglosiewicz, D. Sadiq, J. Shirdel, J. S. Lee, P. Vasa, N. Park, D. S. Kim and C. Lienau, *ACS Nano*, 2012, **6**, 6040–6048.
37 S. Jiang, X. B. Zhang, Y. Zhang, C. R. Hu, R. Zhang, Y. Zhang, Y. Liao, Z. J. Smith, Z. C. Dong and J. G. Hou, *Light: Sci. Appl.*, 2017, **6**, e17098.
38 F. De Angelis, G. Das, P. Candeloro, M. Patrini, M. Galli, A. Bek, M. Lazzarino, I. Maksymov, C. Liberale, L. C. Andreani and E. Di Fabrizio, *Nat. Nanotechnol.*, 2010, **5**, 67–72.
39 F. De Angelis, F. Gentile, F. Mecarini, G. Das, M. Moretti, P. Candeloro, M. L. Coluccio, G. Cojoc, A. Accardo, C. Liberale, R. P. Zaccaria, G. Perozziello, L. Tirinato, A. Toma, G. Cuda, R. Cingolani and E. Di Fabrizio, *Nat. Photonics*, 2011, **5**, 683–688.
40 F. Benz, M. K. Schmidt, A. Dreismann, R. Chikkaraddy, Y. Zhang, A. Demetriadou, C. Carnegie, H. Ohadi, B. de Nijs, R. Esteban, J. Aizpurua and J. J. Baumberg, *Science*, 2016, **354**, 726–729.
41 G. Lu, H. De Keersmaecker, L. Su, B. Kenens, S. Rocha, E. Fron, C. Chen, P. Van Dorpe, H. Mizuno, J. Hofkens, J. A. Hutchison and H. Uji-i, *Adv. Mater.*, 2014, **26**, 5124–5128.
42 H. Ditlbacher, A. Hohenau, D. Wagner, U. Kreibig, M. Rogers, F. Hofer, F. R. Aussenegg and J. R. Krenn, *Phys. Rev. Lett.*, 2005, **95**, 257403.
43 S. Huang, V. Callegari, P. Geisler, C. Brüning, J. Kern, J. C. Prangsma, X. F. Wu, T. Feichtner, J. Ziegler, P. Weinmann, M. Kamp, A. Forchel, P. Biagioni, U. Sennhauser and B. Hecht, *Nat. Commun.*, 2010, **1**, 150.
44 L. Shao, Y. Tao, Q. Ruan, J. Wang and H. Q. Lin, *Phys. Chem. Chem. Phys.*, 2015, **17**, 10861–10870.
45 Y. Lee, N. B. Schade, L. Sun, J. A. Fan, D. R. Bae, M. M. Mariscal, G. Lee, F. Capasso, S. Sacanna, V. N. Manoharan and G. Yi, *ACS Nano*, 2013, **7**, 11064–11070.
46 H. Y. Liang, Z. P. Li, W. Z. Wang, Y. S. Wu and H. X. Xu, *Adv. Mater.*, 2009, **21**, 4614–4618.
47 Y. G. Sun and Y. N. Xia, *Science*, 2002, **298**, 2176–2179.
48 D. Yu and V. W. W. Yam, *J. Am. Chem. Soc.*, 2004, **126**, 13200–13201.
49 C. C. Li, K. L. Shuford, Q. Park, W. P. Cai, Y. Li, E. J. Lee and S. O. Cho, *Angew. Chem., Int. Ed.*, 2007, **119**, 3328–3332.
50 A. Tao, P. Sinsermsuksakul and P. D. Yang, *Angew. Chem., Int. Ed.*, 2006, **45**, 4597–4601.
51 F. Gou and C. J. Murphy, *Chem. Mater.*, 2005, **17**, 3668–3672.
52 H. Y. Liang, H. Wei and H. X. Xu, *Front. Phys.*, 2016, **11**, 45–55.
53 X. Zhuo, X. Zhu, Q. Li, Z. Yang and J. Wang, *ACS Nano*, 2015, **9**, 7523–7535.
54 K. K. Caswell, C. M. Bender and C. J. Murphy, *Nano Lett.*, 2003, **3**, 667–669.
55 Y. G. Sun and Y. N. Xia, *Adv. Mater.*, 2002, **14**, 833–837.
56 S. Kundu and H. Liang, *Adv. Mater.*, 2010, **20**, 826–831.
57 V. A. Zenin, A. Andryieuski, R. Malureanu, I. P. Radko, V. S. Volkov, D. K. Gramotnev, A. V. Lavrinenko and S. I. Bozhevolnyi, *Nano Lett.*, 2015, **15**, 8148–8154.
58 R. Zhang, Y. Zhang, Z. C. Dong, S. Jiang, C. Zhang, L. G. Chen, L. Zhang, Y. Liao, J. Aizpurua, Y. Luo, J. L. Yang and J. G. Hou, *Nature*, 2013, **498**, 82–86.
59 E. J. Bjerneld, K. V. G. K. Murty, J. Prikulis and M. Käll, *ChemPhysChem*, 2002, **3**, 116–119.
60 E. J. Bjerneld, F. Svedberg and M. Käll, *Nano Lett.*, 2003, **3**, 593–596.

61 Y. Niidome, A. Hori, H. Takahashi, Y. Goto and S. Yamada, *Nano Lett.*, 2001, **1**, 365–369.
62 Y. N. Xia, Y. J. Xiong, B. Lim and S. E. Skrabalak, *Angew. Chem., Int. Ed.*, 2009, **48**, 60–103.
63 J. Q. Hu, Q. Chen, Z. X. Xie, G. B. Han, R. H. Wang, B. Ren, Y. Zhang, Z. L. Yang and Z. Q. Tian, *Adv. Funct. Mater.*, 2004, **14**, 183–189.
64 S. H. Zhang, Z. Y. Jiang, Z. X. Xie, X. Xu, R. B. Huang and L. S. Zheng, *J. Phys. Chem. B*, 2005, **109**, 9416–9421.
65 B. Dong, B. S. Cao, Y. Y. He, Z. Liu, Z. P. Li and Z. Q. Feng, *Adv. Mater.*, 2012, **24**, 1987–1993.
66 B. Dong, R. N. Hua, B. S. Cao, Z. P. Li, Y. Y. He, Z. Y. Zhang and O. S. Wolfbeis, *Phys. Chem. Chem. Phys.*, 2014, **16**, 20009–20012.
67 D. Braun and A. Libchaber, *Phys. Rev. Lett.*, 2002, **89**, 188103.
68 S. Chen, Y. J. Zhang, T. Shih, W. M. Yang, S. Hu, X. Y. Hu, J. F. Li, B. Ren, B. W. Mao, Z. L. Yang and Z. Q. Tian, *Nano Lett.*, 2018, **18**, 2209–2216.
69 F. Zhao, W. M. Yang, T. Shih, S. L. Feng, Y. J. Zhang, J. F. Li, J. W. Yan and Z. L. Yang, *ACS Photonics*, 2018, **5**, 3519–1525.
70 A. Lahiri, R. Wen, P. Wang and Y. Fang, *Electrochem. Commun.*, 2012, **17**, 96–99.
71 B. J. Roxworthy, A. M. Bhuiya, S. P. Vanka and K. C. Toussaint, *Nat. Commun.*, 2014, **5**, 3173.
72 Z. P. Li, K. Bao, Y. R. Fang, Y. Z. Huang, P. Nordlander and H. X. Xu, *Nano Lett.*, 2010, **10**, 1831–1835.
73 H. Wei, Z. P. Li, X. R. Tian, Z. X. Wang, F. Z. Cong, N. Liu, S. P. Zhang, P. Nordlander, N. J. Halas and H. X. Xu, *Nano Lett.*, 2011, **11**, 471–475.
74 A. Paul, D. Solis, K. Bao, W. S. Chang, S. Nauert, L. Vidgerman, E. R. Zubarev, P. Nordlander and S. Link, *ACS Nano*, 2012, **6**, 8105–8113.
75 H. Wei, S. P. Zhang, X. R. Tian and H. X. Xu, *Proc. Natl. Acad. Sci. U. S. A.*, 2013, **110**, 4494–4499.
76 S. P. Zhang, H. Wei, K. Bao, U. Håkanson, N. J. Halas, P. Nordlander and H. X. Xu, *Phys. Rev. Lett.*, 2011, **107**, 096801.
77 A. Woessner, M. B. Lundeberg, Y. Gao, A. Principi, P. Alonso-González, M. Carrega, K. Watanabe, T. Taniguchi, G. Vignale, M. Polini, J. Hone, R. Hillenbrand and F. H. L. Koppens, *Nat. Mater.*, 2015, **14**, 421–425.